



# Al-doped ZnO/Ag grid hybrid transparent conductive electrodes fabricated using a low-temperature process



Ha-Rim An<sup>a</sup>, Sung-Tag Oh<sup>a</sup>, Chang Yeoul Kim<sup>b</sup>, Seong-Ho Baek<sup>c</sup>, Il-Kyu Park<sup>d,\*</sup>, Hyo-Jin Ahn<sup>a,\*</sup>

<sup>a</sup> Department of Materials Science & Engineering, Seoul National University of Science and Technology, Seoul 139-743, Republic of Korea

<sup>b</sup> Future Convergence Ceramic Division, Korea Institute Ceramic Engineering and Technology (KICET), Seoul 233-5, Republic of Korea

<sup>c</sup> Energy Research Division, Daegu Gyeongbuk Institute of Science & Technology (DGIST), Daegu 711-873, Republic of Korea

<sup>d</sup> Department of Electronic Engineering, Yeungnam University, Gyeongbuk 712-749, Republic of Korea

## ARTICLE INFO

### Article history:

Received 22 April 2014

Received in revised form 24 June 2014

Accepted 24 June 2014

Available online 2 July 2014

### Keywords:

Transparent conductive electrode

Electrohydrodynamic jet printing

Atomic layer deposition

Ag grid

Al-doped ZnO

## ABSTRACT

Al-doped ZnO (AZO)/Ag grid hybrid transparent conductive electrode (TCE) structures were fabricated at a low temperature by using electrohydrodynamic jet printing for the Ag grids and atomic layer deposition for the AZO layers. The structural investigations showed that the AZO/Ag grid hybrid structures consisted of Ag grid lines formed by Ag particles and the AZO layer covering the inter-spacing between the Ag grid lines. The Ag particles comprising the Ag grid lines were also capped by thin AZO layers, and the coverage of the AZO layers was increased with increasing the thickness of the AZO layer. Using the optimum thickness of AZO layer of 70 nm, the hybrid TCE structure showed an electrical resistivity of  $5.45 \times 10^{-5} \Omega \text{ cm}$ , an optical transmittance of 80.80%, and a figure of merit value of  $1.41 \times 10^{-2} \Omega^{-1}$ . The performance enhancement was suggested based on the microstructural investigations on the AZO/Ag grid hybrid structures.

© 2014 Elsevier B.V. All rights reserved.

## 1. Introduction

Transparent conductive electrodes (TCEs) are thin films that possess simultaneously excellent electrical conductivity ( $\rho \leq 10^{-3} \Omega \text{ cm}$ ) and high visible light wavelength transparency ( $\sim 80\%$ ) [1]. These properties are essential for applications in optoelectronic devices such as flat panel displays, infrared reflectors, light-emitting diodes, and solar cells [2,3]. For these reasons, doped metal oxides, such as ITO ( $\text{Sn}:\text{In}_2\text{O}_3$ ), FTO ( $\text{F}:\text{SnO}_2$ ), AZO ( $\text{Al}:\text{ZnO}$ ) have been the most widely used materials for TCEs because of their high electrical conductivity and transmittance [1]. However, for flexible and bendable electronic or optoelectronic devices, doped metal oxides are not good candidates for TCEs because of their brittle nature [4]. Therefore, alternative TCEs, including thin metal films using noble metals of Au, Ag and Cu, metal grids such as Ag, Cu, and Al grids, and conducting polymers like PEDOT:PSS, have been suggested for flexible device applications [4–6]. However, these structures have low electrical conductivity and transmittance. Thin metal films become more transparent as their thickness decreases to nano-levels. The electrical resistance of the films sharply increases by enhanced electron scattering at surfaces and

boundaries of grains due to reduced grain sizes. On the other hand, metal grids comprised of periodic metal lines can decrease the electron scattering because the thickness of the metal lines is greater than that of metal thin films without decreasing the light transparency [6]. Therefore, metal grids have been preferred to metal thin films. Currently, the main synthetic methods used to fabricate metal grids include electrohydrodynamic (EHD) jet printing and roll-to-roll nanoimprinting [7–9]. In particular, EHD jet printing, which is a non-contact technique, has attracted considerable interest because of advantages such as the possibility of high resolution (below 20  $\mu\text{m}$ ) patterning, generation of smaller droplets than the nozzle size by using a high-viscosity solution, and the use of diverse functional inks (e.g., metallic inks, polymers, and biological materials) [10]. Therefore, many researchers have considered EHD jet-printed Ag grids that show electrical conductivity of up to  $\sim 10^7 \text{ S/m}$  and optical transmittance above 80% [9–12]. However, several problems can occur when Ag grids are used as a top electrode of TCEs. They can be vulnerable to local oxidation and melting by direct exposure to air at high temperature, which adversely affects the electrical properties of the TCEs [13]. And, the empty spacing area between the Ag grid lines makes it conflict between the transmittance and electrical conductivity because there is no electrical current flow in the open area between the grids. Enlarging the empty spacing area between the Ag grid lines to increase the optical transmittance can be decreased

\* Corresponding authors. Tel.: +82 53 810 3093, +82 2 970 6622; fax: +82 2 973 6657.

E-mail addresses: [ikpark@ynu.ac.kr](mailto:ikpark@ynu.ac.kr) (I.-K. Park), [hjahn@seoultech.ac.kr](mailto:hjahn@seoultech.ac.kr) (H.-J. Ahn).

the electrical conductivity. To circumvent these problems, several hybrid TCE structures combining Ag grids with above-mentioned doped metal oxides or conducting polymers have been suggested. In particular, we propose the hybrid TCE structures combining Ag grids and Al-doped ZnO (AZO) thin layers. AZO thin films made by atomic layer deposition (ALD) were chosen as a protective and transparent conductive electrode between grids due to the advantages of AZO such as a wide band gap ( $\sim 3.2$  eV), cheapness, high electrical conductivity, high optical transmittance, and easily controlling electrical and optical properties by doping [14]. AZO thin films made by ALD have shown good electrical properties, electrical resistivity, and carrier concentration [14,15]. In the present study, AZO thin films with different thicknesses (40, 70, and 110 nm) made by ALD were used as a protective oxide TCE between Ag grids. The hybrid structure of a TCE offers many advantages as a result of the lowest electrical resistivity of the Ag grids and whole-area electrical conductance between grids. This is due to the oxide thin film, the protection of Ag nanoparticles from oxidation and melting by the oxide thin film, and an application to flexible electronic devices due to the low temperature process and very thin oxide thin film layer. The purpose of this study is to determine the optimum AZO thickness of Ag grids in order to obtain the highest electrical conductance and optical transmission.

## 2. Experimental

### 2.1. Experimental methods 80

AZO/Ag grid hybrid TCE structures were fabricated by forming Ag grid lines using EHD jet printing, followed by the deposition of thin AZO layers using an ALD method. Both processes were performed at low temperatures ( $\sim 200$  °C), which could also be applied to flexible devices. Ag grid layers were made using an EHD jet printer (Enjet, Suwon, Korea). Ag inks were comprised of Ag nano-sized inks (86%), polyvinylpyrrolidone (PVP, 1300 k, Sigam-Aldrich), and 2 ethoxyethanol as a solvent. The ratio of Ag, PVP, and 2 ethoxyethanol was 77.34%, 1%, and 21.66%, respectively. Ag inks were pumped into the EHD nozzle using a syringe pump at 5  $\mu\text{L}/\text{min}$ . Electrical potential was supplied in a range from 1.6 to 2.0 kV. The nozzle velocity was 800 mm/s, and the distance between the nozzle and substrate was 0.2 mm. AZO thin films were deposited on the Ag metal grids by using an ALD system. Diethylzinc (DEZn), trimethylaluminum (TMAI), and  $\text{H}_2\text{O}$  were used as precursors for the deposition of AZO. The separated precursors were injected into a growth chamber by employing a high-purity  $\text{N}_2$  purge gas to remove residues and products during the deposition. The cycle ratio of DEZn/TMAI was 19:1 and the substrate temperature was fixed at 200 °C. The thickness of the AZO film was controlled by varying the number of source injection cycles. To investigate the optimum conditions for the AZO/Ag grid structures, we fabricated AZO layers on Ag grids with thicknesses of 40, 70, and 110 nm [15]. The AZO/Ag grid hybrid structures with AZO thicknesses of 40, 70, and 110 nm are hereafter referred to as sample A, B, and C, respectively.

### 2.2. Characterizations 102

The structural and morphological properties of AZO/Ag grid hybrid structures were investigated by using X-ray diffraction (XRD, Rigaku X-ray diffractometer equipped with  $\text{Cu K}\alpha$  radiation), field-emission scanning electron microscopy (FE-SEM, Hitachi S-4700), and atomic force microscopy (AFM, diDimension™ 3100). The optical transmittance and electrical properties of the AZO/Ag thin films were characterized using a UV-vis spectrophotometer (Scinco, S-3100) and a Hall effect measurement system (Ecopia, HMS-3000), respectively.

## 3. Results and discussion

Fig. 1 shows XRD data for samples A, B, and C. For all the samples, the main diffraction peaks were observed at  $38.12^\circ$  and  $44.40^\circ$ , corresponding to the (111) and (200) planes, respectively, of a face-centered cubic crystal structure of the Ag phases (Fm3m [225], JCPDS No. 87-0720) from the Ag metal grids. We note that the additional peaks at  $31.82^\circ$ ,  $34.44^\circ$ ,  $36.40^\circ$ , and  $56.72^\circ$  are clearly revealed as the thickness of the AZO thin films on the Ag metal grids increases. These peaks correspond to the (100), (002), (101), and (110) planes of a hexagonal wurtzite structure

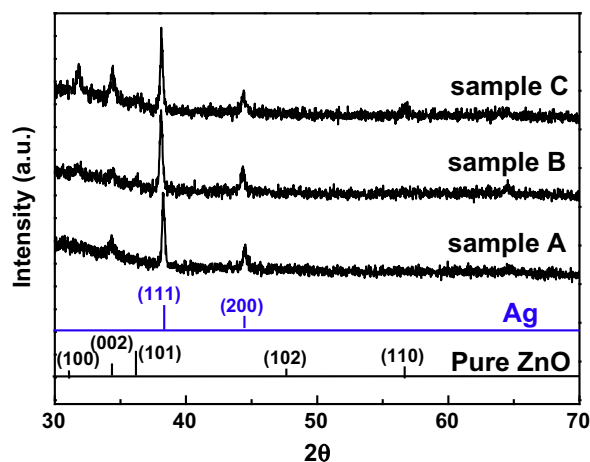


Fig. 1. X-ray diffraction patterns of AZO/Ag grid structures with different AZO layer thicknesses.

of the ZnO phases (space group  $P6_3mc$  [186], JCPDS No. 80-0075). Especially, the observed peaks from the AZO shifted slightly to the higher angle ( $2\theta$ ) compared with those of the ZnO. This can be explained by Bragg's law ( $n\lambda = 2d \sin\theta$ ), and indicates that the lattice distance decreases due to the incorporation of Al into the ZnO lattice because the ionic radius of  $\text{Al}^{3+}$  (0.53 Å) is smaller than that of  $\text{Zn}^{2+}$  (0.74 Å). No additional peaks corresponding to the formation of intermetallic compounds between Ag and AZO were found. This result implies the successful formation of the AZO/Ag grid hybrid structures. 126

Fig. 2(a)–(c) shows the top view FE-SEM images of samples A, B, and C. The surfaces of the samples were clean and composed of Ag grids with a width and pitch of 15 and 450  $\mu\text{m}$ , respectively. Fig. 2(d)–(f) shows microstructural images of the AZO surfaces on the interspacing flat area between the Ag grid lines for samples A, B, and C. Fig. 2(g)–(i) shows cross-sectional images of the Ag grid lines for the samples. The Ag grids are composed of Ag particles with a size range between 163 and 246 nm. Also, the thickness of the Ag metal grids was around 700 nm for the samples. Fig. 2(j)–(l) shows the microstructure of the boundary layer surface between the Ag grid lines and a flat AZO surface. We note that the interspacing between the Ag particles constituting the Ag grid lines is filled with AZO material. The interconnection between the AZO layer and Ag particles was improved with increasing the AZO thickness. As the thickness of the AZO thin films increased, the gaps between the Ag particles filled more densely, resulting in an improved interconnection between the Ag particles. For sample A, the Ag particles and Ag grids are partially covered by AZO material as shown in Fig. 2(j). This results in poor electrical conduction. However, samples B and C show that the Ag grids are completely covered by AZO, as shown in Fig. 2(k) and (l), which result in better electrical conduction of the hybrid thin films.

To investigate the surface morphologies of the Ag grid lines after depositing the AZO layers, we measured the AFM on the Ag grid lines as shown in Fig. 3. The root mean square (RMS) roughness of samples A, B, and C are 38.0, 26.5, and 19.0 Å, respectively. The surface roughness of the Ag grids covered by AZO thin films decreased with increased thickness of the AZO layers. This result could be due to the decreased inter-grain boundary layers between the Ag particles as the AZO thin films covering the Ag particles on the Ag grids. The decrease in inter-grain boundaries could affect the electrical properties of the AZO/Ag grid hybrid structure by improving the electrical conduction.

Fig. 4 shows TEM images of a selected area around the Ag particles for sample B. The sample for TEM measurement was

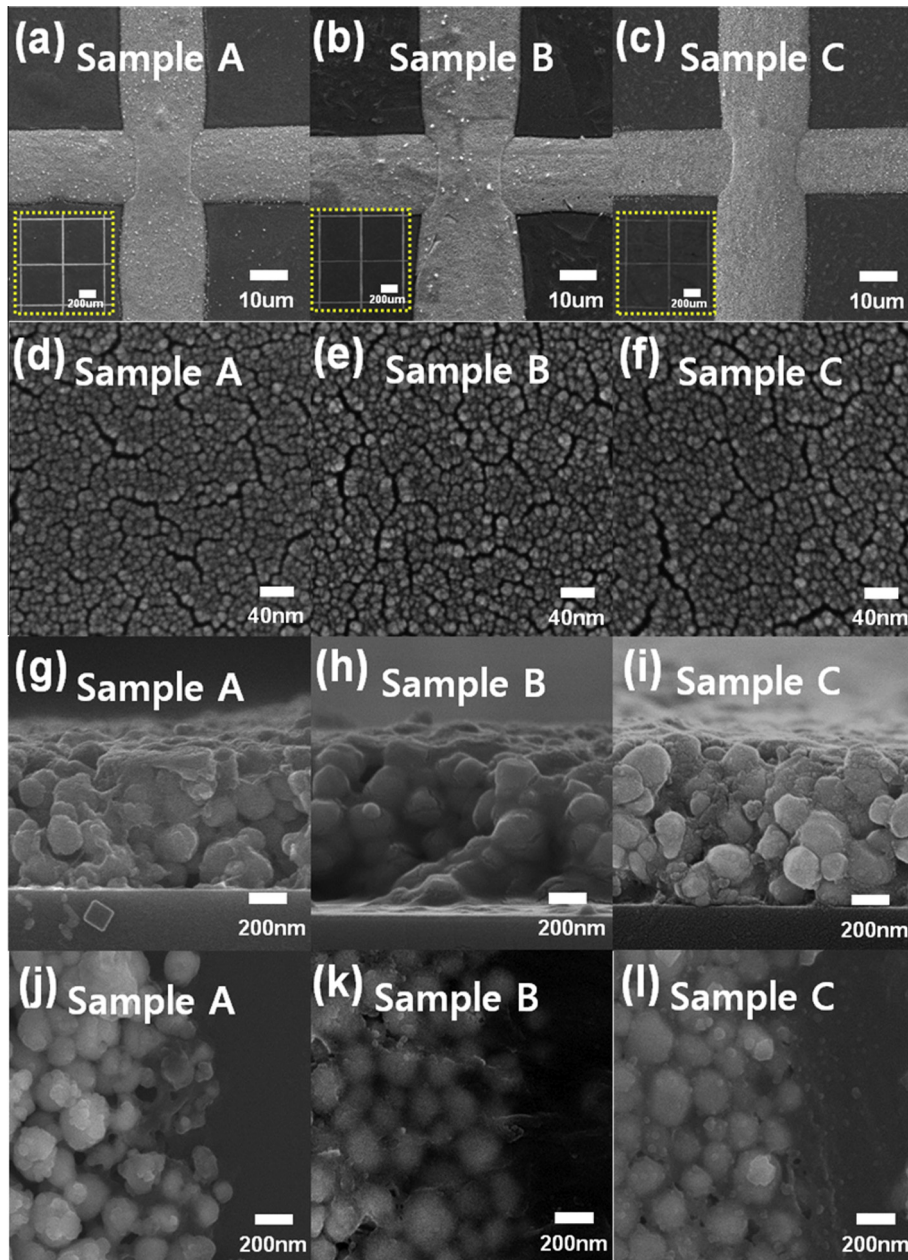


**Fig. 2.** (a)–(c) Top view of FE-SEM images of AZO/Ag grid structure. (d)–(f) AZO surface on the interspacing between the Ag grid lines. (g)–(i) Cross-sectional FE-SEM images of Ag grid lines. (j)–(l) Top view of FE-SEM images of the boundary of AZO and Ag grid lines.

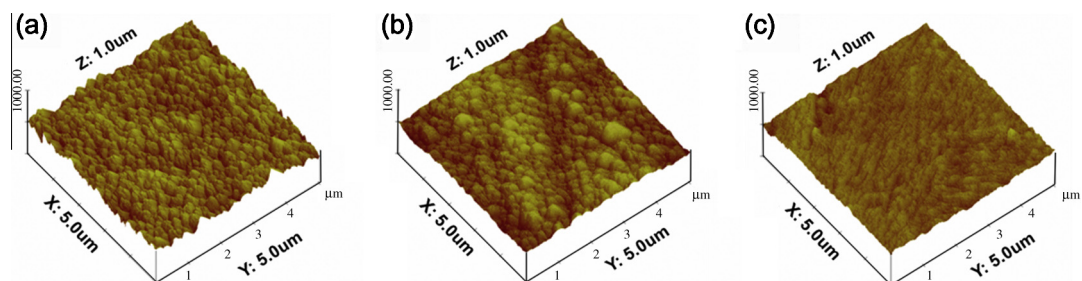


**Fig. 3.** AFM images measured on Ag grid lines covered by AZO thin layers: (a) sample A, (b) sample B, and (c) sample C.

prepared by scraping the surface of sample B, dispersing the samples in ethanol, and placing it on a TEM Cu-grid. The dark region in the TEM image indicates Ag particles, and the surrounding

bright area is an AZO layer. The enlarged image shows that the atomic planes are well developed and composed of polycrystalline domains in the area of the AZO layer, even though the AZO was

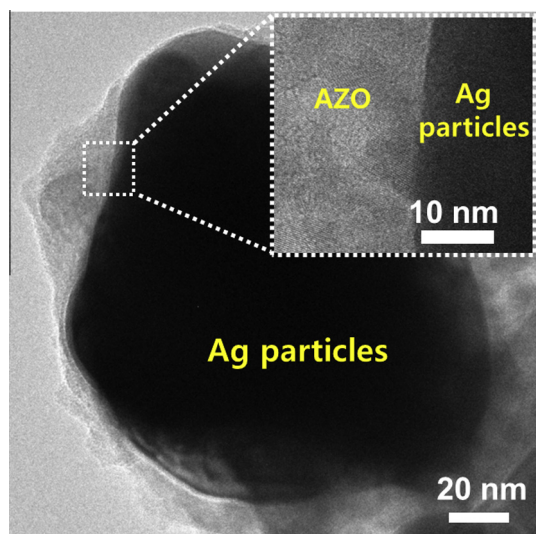


Fig. 4. TEM images of the AZO/Ag grid hybrid structures for sample B.

deposited at a low temperature of 200 °C. A thin AZO layer also partially covers the surface of the Ag particles, which implies that the AZO and Ag particles are well-interconnected. This results in improved electrical conduction between the Ag particles.

The electrical properties of the AZO/Ag grid hybrid structure with different AZO thickness are summarized in Table 1 and Fig. 5. The electrical properties of sample A could not be measured by a Hall effect measurement system because of poor electric conduction. This is because the Ag grid lines were not connected by AZO thin films, thereby resulting in a discontinuous electric current path as shown in Fig. 2(j). However, the interconnection between the AZO and Ag grid lines were improved for samples B and C as shown in Fig. 2(k) and (l), respectively. The carrier concentration was gradually increased from  $3.11 \times 10^{21}$  to  $4.94 \times 10^{21} \text{ cm}^{-3}$  as the thickness of the AZO thin layers increased from 70 to 110 nm. This can be explained by enhanced crystallinity depending on thickness of the films. Films consisting of a few atomic layers of disordered atoms exhibit poor crystallinity, which generates many defects that impede the mobile carriers. However, as the thickness of the films increased, the enhanced crystallinity can increase the concentration of mobile carriers [16]. The Hall mobility of sample B showed a much higher value ( $36.7 \text{ cm}^2/\text{Vs}$ ) than that of sample C ( $3.31 \text{ cm}^2/\text{Vs}$ ). Our previous results showed that AZO thin films deposited by an ALD system without Ag metal grids exhibited Hall mobility values varying from 1.59 to  $3.28 \text{ cm}^2/\text{Vs}$  for AZO thin films with thicknesses ranging from 50 to 150 nm [14]. The Hall mobility of the AZO/Ag grid hybrid structure increased compared to that of the AZO thin films because the electrons could transport through the Ag metal grid lines. This indicates that the Hall mobility of the AZO/Ag grid hybrid structure can be increased by the introduction of Ag metal grid lines as an electron transport path, compared to that of the AZO thin films. Sample C exhibited a reduced mobility value,  $3.31 \text{ cm}^2/\text{Vs}$ , which is similar to those of the AZO thin films without Ag grids. Based on the measured carrier concentration and Hall mobility, the

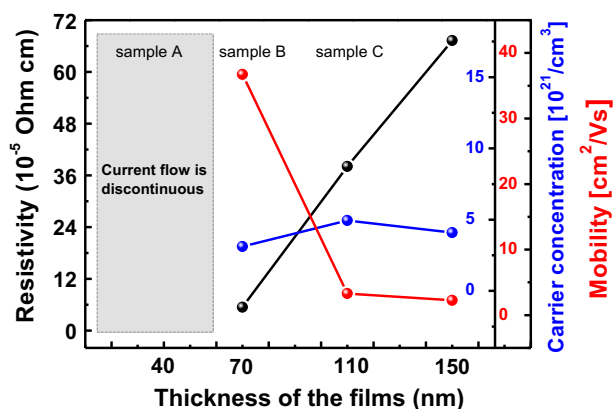


Fig. 5. Electrical properties of AZO/Ag grid hybrid structures with variation in the thickness of the AZO layers.

resistivity ( $\rho$ ) of the hybrid TCEs can be calculated using the following equation [17]:

$$\rho = 1/(Ne\mu)$$

where  $N$  is the carrier concentration,  $\mu$  is the Hall mobility, and  $e$  is the electron unit charge ( $1.602 \times 10^{-19} \text{ C}$ ). The resistivity of samples B and C is  $\sim 5.45 \times 10^{-5}$  and  $\sim 3.81 \times 10^{-4} \Omega \text{ cm}$ , respectively. Sample B showed the lowest resistivity because of the optimum AZO thickness of the hybrid TCEs. Further increase of the AZO thickness up to 150 nm resulted in linearly increased resistivity value to  $6.73 \times 10^{-4} \Omega \text{ cm}$  as shown in Fig. 5. This value is similar range with that of the AZO thin film without Ag grid [14]. This indicates that the electrical properties of the AZO/Ag grid hybrid structure corresponds to that of the AZO thin film itself and the effect of Ag grid on electrical properties are negligibly small as the thickness of the AZO layer increases up to 110 nm.

To investigate the variation of the electrical properties of the hybrid TCEs depending on the thickness of the AZO thin film, microstructure schematic and equivalent circuits of the hybrid TCEs were drawn based on the microstructural and electrical investigations as shown in Fig. 6. Considering the structure of the hybrid TCEs in our structures, current can flow mainly through the Ag grid lines ( $R_{Ag}$ ) and partially through the AZO thin layer ( $R_{AZO}$ ) between the Ag grid lines. Depending on the thickness of AZO thin film, the interconnection between the Ag grids and AZO thin film in the spacer layer, and the interconnection between the Ag particles within the Ag grid lines, can be varied as verified in the microstructural investigations. In the case of sample A or the case without the AZO layers, the current path is only the Ag grid line because of the extremely large resistance of the thin AZO layers. Ag particles consisting of Ag grid lines are not fully connected to each other. Therefore, electrons can be scattered at the boundary between the Ag particles, resulting in high electrical resistance. For the AZO layer with optimum thickness (sample B), the current path can be divided into two parts: the Ag grid lines and an AZO layer. In this case, the electrical conduction through both paths can be improved at the same time due to the AZO layer. Because the interconnection between the Ag grid lines and the AZO

Table 1  
Summary of electrical and optical properties of the AZO/Ag grid hybrid structures.

Sample	Carrier concentration ( $\text{cm}^{-3}$ )	Hall mobility ( $\text{cm}^2/\text{Vs}$ )	Resistivity ( $\Omega \text{ cm}$ )	Average transmittance (%)
A	–	–	–	83.04
B	$3.11 \times 10^{21}$	36.74	$5.45 \times 10^{-5}$	80.80
C	$4.94 \times 10^{21}$	3.31	$3.81 \times 10^{-4}$	80.15

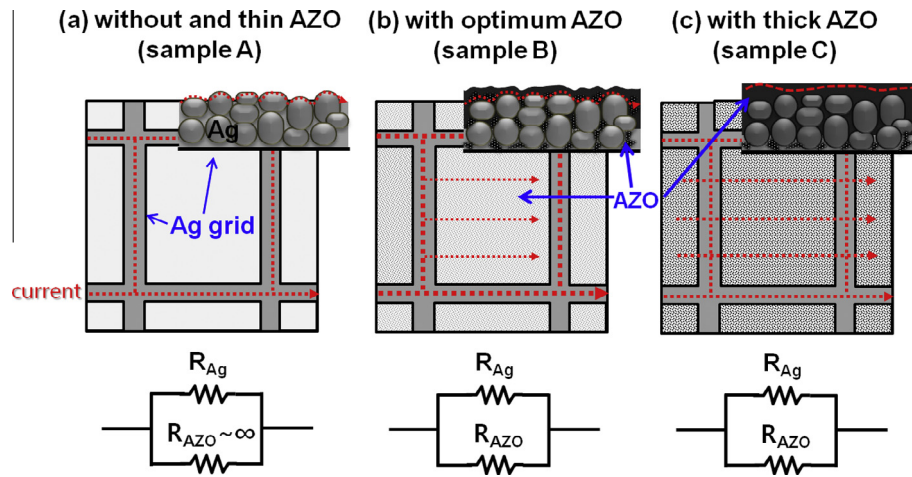


Fig. 6. Schematics of microstructures and an equivalent circuit diagram of AZO/Ag grid hybrid structures with variation in the thickness of the AZO layer.

layer are improved, the resistance of the AZO layer is reduced due to increased thickness, the total resistance through the AZO layer ( $R_{AZO}$ ) can be reduced. Furthermore, the resistance of the Ag grid lines ( $R_{Ag}$ ) can be reduced because the AZO partially fills the gaps between the Ag particles that act to block the electron flow. Therefore, the electrical properties of the hybrid TCE with an optimum AZO layer can be improved. However, with even thicker AZO layers (sample C), the electrical resistance through the main path of the Ag grid can be increased because the Ag particles are completely covered by the AZO layer, as shown in Figs. 2(l) and 6(c). Therefore, to design a hybrid TCE, the microstructural properties of the materials used should be understood, and this is crucial in designing hybrid TCE structures with excellent electrical properties.

Fig. 7(a) shows optical properties obtained from samples A, B, and C. The average optical transmittances in the visible range ( $\sim 550$  nm) are 83.0, 80.8, and 80.1% for samples A, B, and C, respectively. The transmittance decreases with an increase in the AZO layer thickness because of the increase of the absorbing medium (i.e., the AZO layer). We note that all hybrid TCEs fabricated in this study showed a high average transmittance value (over 80%) in the visible range, remaining the electrical resistivity much lower than  $10^{-3} \Omega \text{ cm}$  at the same time, which indicates that the proposed hybrid structure could be a good candidate for use in TCEs. To investigate the optical properties further, the optical bandgap energy ( $E_{opt}$ ) of the TCEs was estimated using the following equation [18]:

$$(\alpha h\nu)^2 = A(h\nu - E_{opt})$$

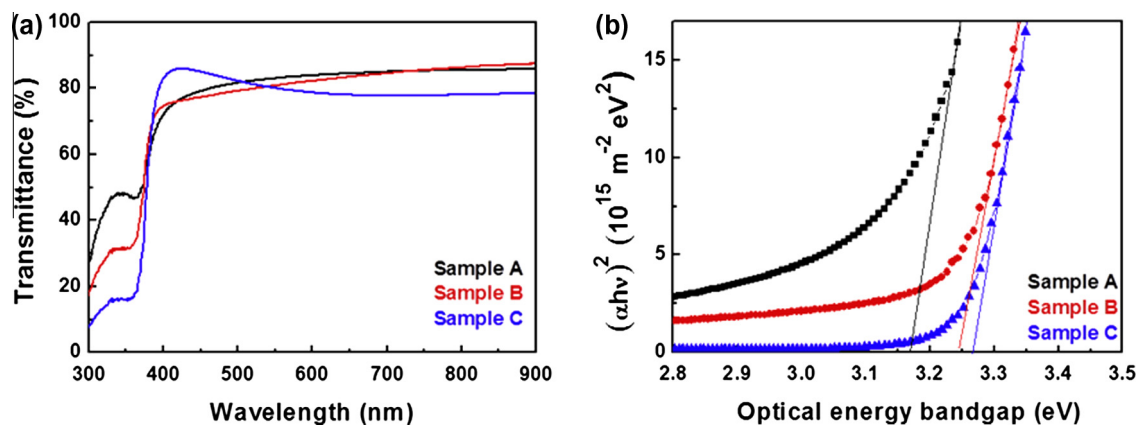


Fig. 7. (a) Optical transmission spectra and (b) plots of  $(\alpha h\nu)^2$  versus  $h\nu$  for the AZO/Ag grid hybrid structures with variation of the thickness of AZO layers.

where  $\alpha$  is the absorption coefficient assumed by  $\alpha = (1/d)\ln(1/T)$ , where  $T$  is the transmittance,  $d$  is the film thickness,  $A$  is a constant for a direct transition,  $h$  is Planck's constant, and  $\nu$  is the frequency of the incident photon. From Fig. 7(b), the  $E_{opt}$  values for samples A, B, and C were estimated to be 3.17, 3.24, and 3.26 eV, respectively. The  $E_{opt}$  value of sample A is slightly lower than that of pure ZnO (3.2 eV), and the  $E_{opt}$  values of samples B and C are slightly higher than that of undoped ZnO. This could be explained by the Burstein-Moss effect, which occurs when the carrier concentration exceeds the density of state in the conduction band edge, and the optical band gap is extended.

To evaluate the performance of AZO/Ag grids, the figure of merit (FOM) of the TCEs was calculated using the following equation [19]:

$$FOM = T^{10}/R_s$$

where  $T$  is the optical transmittance and  $R_s$  is the sheet resistance. The FOM values were calculated to be  $\sim 1.52 \times 10^{-2} \Omega^{-1}$  for sample B and  $\sim 3.14 \times 10^{-3} \Omega^{-1}$  for sample C. This implies that the optimum thickness of the AZO thin layers covering the Ag metal grids results in excellent electrical properties of the hybrid TCEs without degrading the optical transmittance. Comparing with the reported FOM values of TCEs fabricated by other processes such as sputtering, spray pyrolysis, and pulsed laser deposition, the values in the range of  $\sim 2.5 \times 10^{-3} \Omega^{-1}$  to  $2.8 \times 10^{-2} \Omega^{-1}$  [20–22], the AZO/Ag grid hybrid TCEs fabricated by EHD jet printing and ALD in this study exhibited superior electrical and optical properties for use in various optoelectronic devices. This is due to the advantages of

the ALD system, which provides conformal coating of the deposits even on complicated structures because of a long mean free path, and fewer gas phase reactions of the sources in ALD systems [23].

#### 4. Conclusions

In summary, we fabricated AZO/Ag grid hybrid TCE structures at a low temperature by using a combination of the EHD jet printing method and the ALD method. Structural investigations using XRD, FE-SEM, and AFM showed that the AZO/Ag grid hybrid structures exhibit an AZO layer covered the inter-spacing between the Ag grid lines. Furthermore, the Ag particles comprising the Ag grid lines were covered by thin AZO layers that affected the electrical conduction. The coverage of the AZO layers increased with the increasing thickness of the AZO layer. Using the optimum thickness of the AZO layer (70 nm), the hybrid TCE structure showed superior electrical resistivity ( $\sim 5.45 \times 10^{-5} \Omega \text{ cm}$ ), good optical transmittance ( $\sim 80.80\%$ ), and a superior FOM ( $\sim 1.52 \times 10^{-2} \Omega^{-1}$ ). We examined the performance enhancement mechanism based on the microstructural evolution of the AZO/Ag grid hybrid structures. Our findings, which can be applied to various flexible device applications in displays and solar cells, can provide critical clues for designing high performance TCEs.

#### Acknowledgements

This work was supported by Grant No. 10041161 from the Ministry of Knowledge Economy (MKE) and Fundamental R&D Program for Core Technology of Materials funded by the Ministry of Knowledge Economy, Republic of Korea.

#### References

- [1] T. Minami, *Semicond. Sci. Technol.* 20 (2005) S35–S44.
- [2] N.L.H. Hoang, N. Yamada, T. Hitosugi, J. Kasai, S. Nakao, T. Shimada, T. Hasegawa, *Appl. Phys. Express* 1 (2008) 115001.
- [3] A. Hongsingthong, T. Krajangsang, I.A. Yunaz, S. Miyajima, M. Konagai, *Appl. Phys. Express* 3 (2010) 051102.
- [4] S. De, T.M. Higgins, P.E. Lyons, E.M. Doherty, P.N. Nirmalraj, W.J. Blau, J.J. Boland, J.N. Coleman, *ACS Nano* 3 (2009) 1767–1774.
- [5] J. Zou, H.L. Yip, S.K. Hau, A.Y. Jen, *Appl. Phys. Lett.* 96 (2010) 203301.
- [6] L.B. Hu, H. Wu, Y. Cui, *MRS Bull* 36 (2011) 760–765.
- [7] M.G. Kang, H.J. Park, S.H. Ahn, T. Xu, L.J. Guo, *IEEE J. Sel. Top. Quant. Electron.* 16 (2010) 1807–1820.
- [8] S.H. Ahn, L.J. Guo, *Nano Lett.* 10 (2010) 4228–4234.
- [9] Y.H. Jang, J.H. Kim, D.Y. Byun, *J. Phys. D: Appl. Phys.* 46 (2013) 155103.
- [10] E. Sutanto, K. Shigeta, Y.K. Kim, P.G. Graf, D.J. Hoelzle, K.L. Barton, A.G. Alleyne, P.M. Ferreira, J.A. Rogers, *J. Micromech. Microeng.* 22 (2012) 045008.
- [11] D.H. Youn, S.H. Kim, Y.S. Yang, S.C. Lim, S.J. Kim, S.H. Ahn, H.S. Sim, S.M. Ryu, D.W. Shin, J.B. Yoo, *Appl. Phys. A* 96 (2009) 933–938.
- [12] C.H. Liu, Xun Yu, *Nanoscale Res. Lett.* 6 (2011) 75.
- [13] A.R. Kim, Y.L. Won, K.H. Woo, C.H. Kim, J.H. Moon, *ACS Nano* 7 (2013) 1081–1091.
- [14] H.R. An, S.H. Baek, I.K. Park, H.J. Ahn, *Korean J. Mater. Res* 23 (2013) 469–475.
- [15] H.K. Park, B.S. Yang, S. Park, M.S. Kim, J.C. Shin, J. Heo, *J. Alloys Comp.* 605 (2014) 124–130.
- [16] C.C. Kuo, C.C. Liu, S.C. He, J.T. Chang, J.L. He, *J. Nanomater.* 2011 (2011) Article ID 140697.
- [17] S. Calnan, A.N. Tiwari, *Thin Solid Films* 518 (2010) 1839–1849.
- [18] M. Wang, K.E. Lee, S.H. Hahn, E.J. Kim, S. Kim, J.S. Chung, E.W. Shin, C.H. Park, *Mater. Lett.* 61 (2007) 1118–1121.
- [19] J. Liu, A.W. Hains, J.D. Servaites, M.A. Ratner, T.J. Marks, *Chem. Mater.* 21 (2009) 5258–5263.
- [20] S.M. Park, T. Ikegami, K.J. Ebihara, *Jpn. J. Appl. Phys* 45 (2006) 8453–8456.
- [21] S.S. Lin, J.L. Huang, *Ceram. Int.* 30 (2004) 497–501.
- [22] M.N. Islam, B.K. Samantaray, K.L. Chopra, H.N. Acharya, *Sol. Energy Mater. Sol. Cells* 29 (1993) 27–35.
- [23] B.Y. Noh, S.H. Baek, Y.I. Jung, J.H. Kim, I.K. Park, *J. Nanosci. Nanotechnol.* 13 (2013) 3335–3340.